Experimental and theoretical study of the magnetic and structural properties of $Er_{0.75}Tb_{0.25}Al_2$

Mahmud Khan, Ya. Mudryk, and D. Paudyal
The Ames Laboratory, U.S. Department of Energy, Iowa State University, Ames, Iowa 50011-3020, USA

K. A. Gschneidner, Jr. and V. K. Pecharsky
The Ames Laboratory, U.S. Department of Energy, Iowa State University, Ames, Iowa 50011-3020, USA
and Department of Materials Science and Engineering, Iowa State University, Ames, Iowa 50011-2300, USA
(Received 14 May 2010; revised manuscript received 21 July 2010; published 20 August 2010)

The $Er_{0.75}Tb_{0.25}Al_2$ alloy has been investigated by x-ray powder diffraction, magnetization, and ac magnetic-susceptibility measurements. The low-field magnetization measured as a function of temperature indicates a ferromagnetic transition at ~36 K and another transition with thermal hysteresis at ~18 K. The ac magnetic-susceptibility measurements show frequency dependence below the ferromagnetic transition temperature, T_C. Low-temperature x-ray powder-diffraction measurements suggest that although no structural transformation occurs around 18 K, a steplike anomaly in the lattice parameters does exist in the vicinity of the transition. First-principles electronic-structure calculations show anomalous density of states at the Fermi level. The results are comparable with the previously reported $Er_{0.75}Dy_{0.25}Al_2$ alloy, thus supporting an earlier assumption that mixing two rare-earth ions with opposite signs of second-order Steven's factor in RAl_2 alloys creates a competition between the magnetoelastic and quadrupolar interactions, giving rise to multiple magnetic ordering phenomena.

DOI: 10.1103/PhysRevB.82.064421 PACS number(s): 75.50.Cc, 71.20.Lp, 75.80.+q

I. INTRODUCTION

The $MgCu_2$-type cubic Laves phase RAl_2 (R=rare earth) compounds are among many rare-earth compounds that have been broadly studied in the past for their interesting fundamental and potentially important applied properties, such as magnetostriction,[1] strong magnetocaloric effect,[2–4] large magnetoresistance,[5] and other. With the exception of $LaAl_2$, $YbAl_2$, $LuAl_2$, and $EuAl_2$, all RAl_2 compounds order ferromagnetically below their respective Curie temperatures, T_C.[6] The ferromagnetism in these compounds is localized on the R^{3+} sites and no magnetic contributions are made by Al.[7] Since the RAl_2 compounds are isostructural, and the R^{3+} ions are responsible for the magnetic moments, these Laves phases are considered model systems for study of crystalline electric field effects in rare-earth compounds.[8]

Although the RAl_2 compounds share many common properties, some of the members in the series exhibit features that are quite unique. For example, $HoAl_2$ undergoes a first-order spin-reorientation transition in the ferromagnetic state, which is not observed in any other member of the RAl_2 series.[5,9] Spin-reorientation transition also exists in $DyAl_2$, even though it is no longer a first-order transformation.[10]

The $4f$ charge densities of the rare-earth atoms that are represented by the second-order Stevens's factors are significantly different.[11] Due to this reason, interesting phenomena may occur when one type of R atom in RAl_2 is partially replaced by a different R' atom. When such substitutions are done, properties like T_C, and lattice parameters generally change linearly with the doping concentration x in $R_{1-x}R'_xAl_2$ series.[12,13] In addition to the change in T_C and lattice parameters, interesting phenomenon was observed recently in pseudobinary $Er_{1-x}Dy_xAl_2$ and $Er_{1-x}Tb_xAl_2$ alloys.[14–16]

It has been reported that partial replacement of Er by Dy in $Er_{1-x}Dy_xAl_2$ and by Tb in $Er_{1-x}Tb_xAl_2$ alloys results in multiple magnetic ordering transitions that vary unusually with Dy and Tb concentration. For some critical Dy and Tb concentrations, first-orderlike transitions were observed in the heat-capacity and magnetization data.[14–16] It was shown that the observed behavior is a result of the competition between the magnetoelastic and quadrupolar effects.[14–16] It was also suggested that the modification of the magnetic structure of the $Er_{1-x}Dy_xAl_2$ system is mainly caused by the $4f$ charge densities of Er^{3+} being different from Dy^{3+} and Tb^{3+}. The $4f$ charge density of Er^{3+} is a prolate spheroid, whereas the $4f$ charge densities of Dy^{3+} and Tb^{3+} are shaped as oblate spheroids, i.e., the sign of the second-order Steven's factor of Er^{3+} is opposite to those of Dy^{3+} and Tb^{3+}.[11]

Although the heat capacities of $Er_{1-x}Dy_xAl_2$ and $Er_{1-x}Tb_xAl_2$ alloys exhibit similar behavior, the first-orderlike peaks in the $Er_{1-x}Tb_xAl_2$ alloys are much weaker. The reason for the weaker peaks in $Er_{1-x}Tb_xAl_2$ was attributed to the much smaller magnitude of the second-order Steven's factor for Tb^{3+} ($-1/99$) when compared to that for Dy^{3+} ($-2/9.35$).[16] Regardless of the much smaller magnitude of the second-order Steven's factor of Tb^{3+} compared to Dy^{3+}, the first-order peaks appear around the same concentration, i.e., x=0.25 in both $Er_{1-x}Dy_xAl_2$ and $Er_{1-x}Tb_xAl_2$ alloys. So far the magnetic properties have been reported only for $Er_{1-x}Dy_xAl_2$.[15] It is therefore, interesting to explore the magnetic properties of $Er_{1-x}Tb_xAl_2$, and in this paper we report the magnetic and low-temperature structural properties of $Er_{1-x}Tb_xAl_2$ for x=0.25, and first-principles electronic-structure calculations for x=0.0, 0.25, and 1.

II. EXPERIMENTAL DETAILS

The Tb and Er metals used to prepare the $Er_{0.75}Tb_{0.25}Al_2$ alloy were prepared by the Materials Preparation Center of the Ames Laboratory[17] and were 99.8+ at. % pure with re-

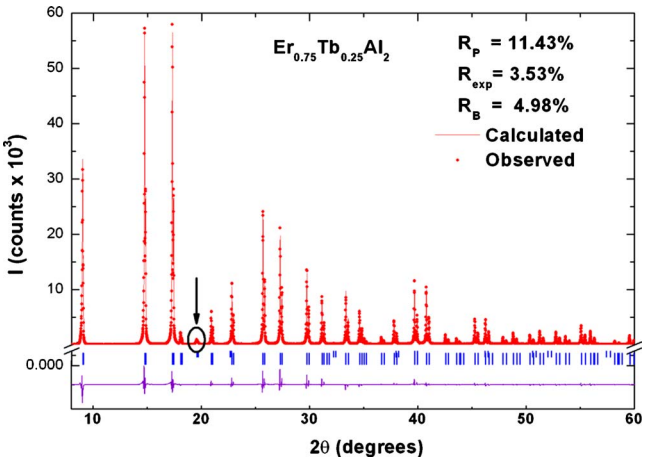

FIG. 1. (Color online) Observed (symbols) and calculated (line drawn through the symbols) room-temperature x-ray powder-diffraction patterns of $Er_{0.75}Tb_{0.25}Al_2$. The difference $I_{obs}-I_{calc}$ is shown at the bottom of the plot. Vertical bars under the patterns indicate calculated positions of Bragg peaks of $Er_{0.75}Tb_{0.25}Al_2$ (larger lower bars) and Cu (shorter upper bars).

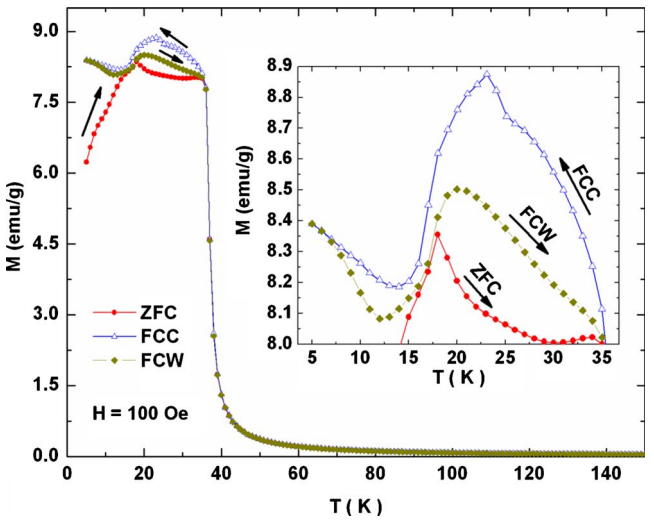

FIG. 2. (Color online) Temperature dependencies of dc magnetization of $Er_{0.75}Tb_{0.25}Al_2$ measured in an applied field of 100 Oe under ZFC, FCC, and FCW conditions. The inset shows the details of the low-temperature region around the transition.

spect to all other elements in the Periodic Table with the following major impurities (in parts per million atomic): Er—C(320), F(62), Fe(263), N(36), O(42), and Tb—C(105), F(37), H(135), N(12), O(199). The Al metal of 5N purity was purchased from Alfa Aesar Inc. A polycrystalline button of $Er_{0.75}Tb_{0.25}Al_2$ alloy weighing approximately 5 g was prepared by conventional arc melting of the stoichiometric mixture of components in an argon atmosphere. To ensure homogeneity the alloy was remelted several times with the button being flipped over after each melting; the weight losses of the sample after melting were less than 0.1%. The alloy melts congruently, and therefore, annealing was not necessary.

To check the phase purity and verify the crystal structure of the sample, x-ray powder diffraction (XRD) analysis was performed on a Rigaku TTRAX rotating anode powder diffractometer employing Mo $K\alpha$ radiation.[18] XRD measurements were also performed at different temperatures using the same diffractometer. The diffractometer is equipped with a continuous flow ^{4}He cryostat controlling the temperature of a sample. For the XRD measurements, the sample was prepared and mounted on a copper sample holder as described in Refs. 18 and 19. The phase and lattice parameters were determined from Rietveld analysis using LHPM Rietica.[20] Both ac and dc magnetic measurements were conducted in a superconducting quantum interference device (SQUID) magnetic property measurement system (MPMS) model XL-7 made by Quantum Design Inc. The measurements were performed in the temperature range of 5–300 K and in applied magnetic fields up to 7 T.

III. RESULTS AND DISCUSSION

A. Room-temperature XRD and magnetization measurements

The room-temperature XRD patterns of $Er_{0.75}Tb_{0.25}Al_2$ are shown in Fig. 1. The alloy adopts the $MgCu_2$-type cubic Laves phase structure at room temperature with the lattice parameter $a=7.82109(3)$ Å. Weak Bragg peaks representing elemental copper are found in the observed XRD pattern (see the circled Bragg peak marked by arrow in Fig. 1). The copper particles contaminating surface came from the copper sample holder used for preparation of the specimen for x-ray powder-diffraction measurements.[18]

Figure 2 shows the dc magnetization, $M(T)$, of $Er_{0.75}Tb_{0.25}Al_2$ measured as a function of temperature in a magnetic field of 100 Oe. Before measuring the zero-field-cooled (ZFC) curve, the sample was cooled from 300 to 5 K in a zero magnetic field. To ensure that the magnetic field is close to zero, a demagnetization sequence (decaying oscillations of the magnetic field around zero) was executed in the SQUID before each ZFC measurement. Regardless of this, it is possible that a very small field of a few oersted was still present during the cooling of the sample for each ZFC measurement. When the temperature reached 5 K, a magnetic field of 100 Oe was applied. Upon the stabilization of the magnetic field the ZFC $M(T)$ data were measured as a function of increasing temperature. The FC cooling (FCC) curve was measured by sweeping down the temperature from 300 to 5 K in an applied field of 100 Oe. The FC warming (FCW) curve was obtained in a similar way to that of the ZFC curve with the exception that the sample was cooled down in the presence of a magnetic field of 100 Oe.

As shown in Fig. 2, the ZFC magnetization initially increases with temperature reaching a peak at ~18 K. After that the magnetization decreases slowly, and at ~36 K a sharp drop of magnetization represents the transition from the ferromagnetic to a paramagnetic state. Above the ferromagnetic transition temperature, $T_C=36$ K, the ZFC, FCC, and FCW curves are identical. However, significant differences including irreversible thermomagnetic behavior are observed below T_C (see inset of Fig. 2). The FCC curve below T_C shows an increase in magnetization with decreasing temperature. The magnetization reaches a peak around

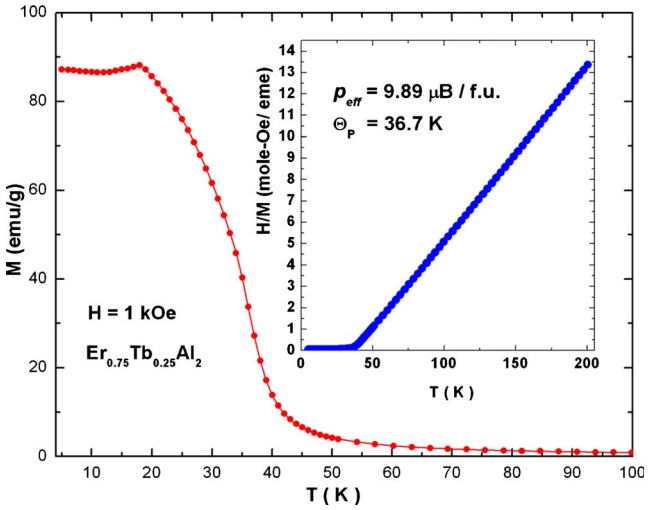

FIG. 3. (Color online) Temperature dependence of dc magnetization of $Er_{0.75}Tb_{0.25}Al_2$ measured in an applied field of 1 kOe under ZFC condition. The inset shows the temperature dependence of the inverse susceptibility (H/M) for a field of 1 kOe.

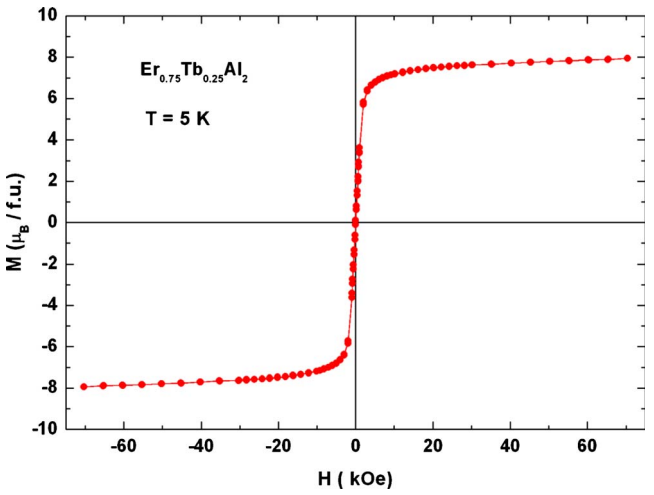

FIG. 4. (Color online) Field dependence of magnetization of $Er_{0.75}Tb_{0.25}Al_2$ measured at 5 K.

23 K and then starts decreasing. Below 14 K, the magnetization starts to increase again. The FCW $M(T)$ curve exhibits similar behavior to that of the FCC curve with lower values of the magnetization. Noticeable hysteresis between the FCC and FCW curves suggest that the transition observed near 18 K is a first-order phase transition. The first-order nature of this transition was also identified in the behavior of heat capacity of the same alloy.[16]

Figure 3 shows the ZFC $M(T)$ curve of $Er_{0.75}Tb_{0.25}Al_2$ measured in a magnetic field of 1 kOe. The inset shows the temperature dependence of the inverse susceptibility (H/M) of the sample. It is evident in the figure that a peak in the $M(T)$ curve exists around 18 K, which is the same temperature where a peak was observed in the ZFC $M(T)$ curve of the sample measured in a 100 Oe field (see Fig. 2). However, unlike the ZFC $M(T)$ curve at 100 Oe, the curve measured at 1 kOe shows that the magnetization does not change much below 18 K. Above T_C, the inverse susceptibility follows the Curie-Weiss behavior. The effective magnetic moment, p_{eff}, and the paramagnetic Weiss temperature, Θ_P, calculated from H/M vs T data are 9.89 μ_B/R^{3+} and 36.7 K, respectively. The expected p_{eff} for a mixture of 0.75 Er+0.25 Tb noninteracting trivalent ions is 9.62 μ_B, which is comparable with the experimental value.

Figure 4 shows the field dependence of magnetization of $Er_{0.75}Tb_{0.25}Al_2$ measured at 5 K. The magnetic moment nearly saturates in 70 kOe magnetic field, and the value of the moment is 7.9 μ_B, which is notably smaller than the expected moment of 9.0 μ_B. The saturation moment of $Er_{0.75}Dy_{0.25}Al_2$ at 2 K was also found to be less than the expected theoretical value.[15] The reduction in the moment was attributed to the crystal-field and magnetic anisotropy effects. The reduction in the magnetic moment in the $Er_{0.75}Tb_{0.25}Al_2$ compound is most probably caused by similar effects.

The results of the magnetic measurements discussed so far are very similar to those observed in $Er_{0.75}Dy_{0.25}Al_2$ with the exception that the transition temperatures observed in $Er_{0.75}Tb_{0.25}Al_2$ are higher. The low-temperature first-orderlike transition in $Er_{0.75}Dy_{0.25}Al_2$ was observed at ~10 K whereas a similar transition is observed in $Er_{0.75}Tb_{0.25}Al_2$ at ~18 K. The Curie temperature of $Er_{0.75}Dy_{0.25}Al_2$ is ~25 K and the Curie temperature of $Er_{0.75}Tb_{0.25}Al_2$ is ~36 K. The difference in the T_C's can be attributed to the differences in the de Gennes factors of the Dy and Tb trivalent ions. The observed similarities in the $M(T)$ curves of $Er_{0.75}Tb_{0.25}Al_2$ and $Er_{0.75}Dy_{0.25}Al_2$, particularly the observed first-orderlike transitions, indicate that as proposed earlier,[14,15] the combination of two R^{3+} ions with opposite signs of the second-order Steven's factors results in multiple magnetic ordering phenomena in alloys under study.

B. ac magnetic susceptibility

ac magnetic-susceptibility measurements of the $Er_{0.75}Tb_{0.25}Al_2$ alloy were performed in an ac field (H_{ac}) of 5 Oe, and at frequencies of 1, 10, 100, and 1000 Hz. The measurements were carried out on heating in the presence of zero dc magnetic field and over the temperature range of 5–60 K. The temperature variations in the real and imaginary components of the ac susceptibility are shown in Figs. 5(a) and 5(b), respectively. As shown in Fig. 5(a), the real component of the ac susceptibility, χ', increases with increasing temperature with a change in slope at 18 K. We recall that at the same temperature, the first-orderlike transition is observed in the $M(T)$ data of the alloy (see Fig. 2). The χ' recorded as a function of temperature at 1 Hz shows a small peak around 18 K, which disappears with the increasing frequency. The peak at 18 K and the slope change are more obvious in the $d\chi'/dT$ vs T curves shown in the upper inset of Fig. 5(a). Above the slope change around 18 K, χ' increases nearly linearly with increasing temperature until it drops sharply at T_C. Weak frequency dependence is observed in the χ' data below T_C. The χ'' data [Fig. 5(b)] measured at a frequency of 1 Hz show a small rounded peak around 8 K and a sharp peak at 18 K, which are followed by a rounded

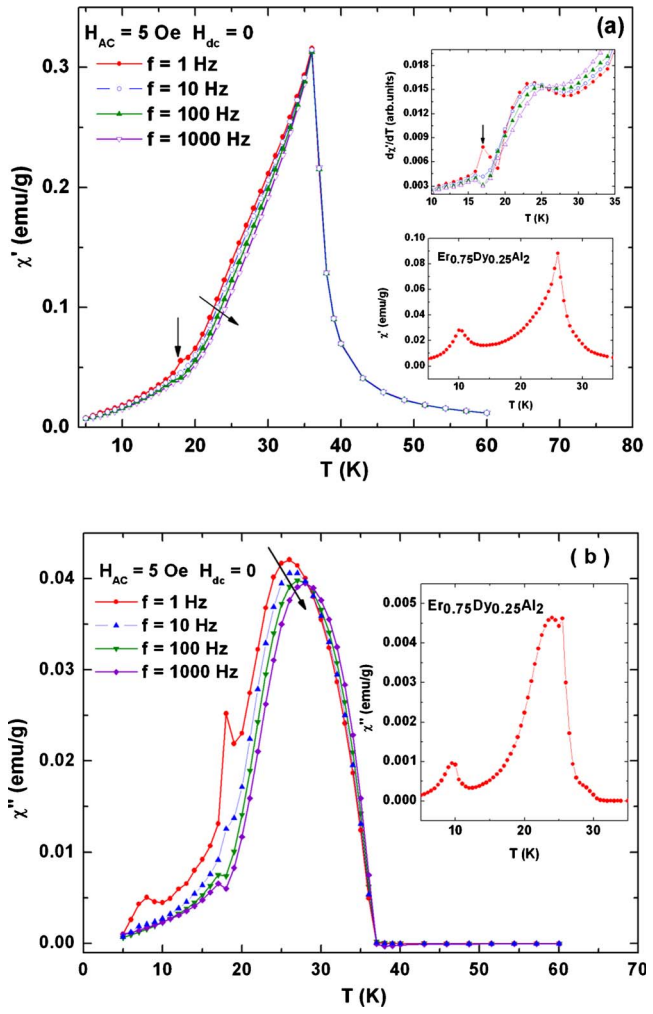

FIG. 5. (Color online) (a) Temperature dependence of real component of the ac magnetic susceptibility of $Er_{0.75}Tb_{0.25}Al_2$ measured in an ac field of 5 Oe and frequencies from 1 to 1000 Hz. The upper inset of Fig. 5(a) shows the derivative of the real component as a function of temperature and lower inset shows the real component of the ac magnetic susceptibility of $Er_{0.75}Dy_{0.25}Al_2$ at a frequency of 1 Hz. (b) Imaginary components of the ac magnetic susceptibility of $Er_{0.75}Tb_{0.25}Al_2$. The inset shows the imaginary component of $Er_{0.75}Dy_{0.25}Al_2$ at 1 Hz.

peak around 26 K. This peak at 26 K shifts to a higher temperature with increasing frequency. The rounded peak at 8 K disappears for frequencies equal to and greater than 10 Hz. The sharp peak at 18 K diminishes with increasing frequency but a weak anomaly is still observed around this temperature even at 1000 Hz.

Although the $M(T)$ curves of $Er_{0.75}Tb_{0.25}Al_2$ and $Er_{0.75}Dy_{0.25}Al_2$ are quite similar, significant differences are observed in the respective ac susceptibilities. The first-orderlike transition around 10 K observed in the $M(T)$ data of $Er_{0.75}Dy_{0.25}Al_2$ corresponds very well with the ac susceptibility data for all frequencies.[15] The χ' and χ'' curves with respect to temperature for $Er_{0.75}Dy_{0.25}Al_2$ measured at a frequency of 1 Hz are shown in the lower insets of Figs. 5(a) and 5(b), respectively. In case of $Er_{0.75}Tb_{0.25}Al_2$ the transition observed around 18 K in the $M(T)$ data is weakly reflected in the χ' data and only for a low (1 Hz) frequency. Further a sharp peak that is observed in the χ'' data at a frequency of 1 Hz is strongly diminished as the frequency is increased, which is not the case in $Er_{0.75}Dy_{0.25}Al_2$. The weaker peaks in the ac susceptibility data of $Er_{0.75}Tb_{0.25}Al_2$ correlate well with the corresponding heat-capacity peaks of the alloy.[16]

The observed similarities and differences in $Er_{0.75}Tb_{0.25}Al_2$ and $Er_{0.75}Dy_{0.25}Al_2$ discussed so far may be explained by considering some differences in the fundamental properties of Tb^{3+} and Dy^{3+} ions, which are believed to be the main reason that causes weaker and sharper anomalies in the heat capacities of $Er_{1-x}Tb_xAl_2$ and $Er_{1-x}Dy_xAl_2$, respectively.[16] As mentioned earlier, the low-temperature first-orderlike transition in $Er_{0.75}Dy_{0.25}Al_2$ was attributed to the opposite signs of the second-order Steven's factors of Er^{3+} and Dy^{3+} ions. Due to this difference, competition arises between the quadrupolar and magnetoelastic interactions that modify the magnetic structure of $Er_{0.75}Dy_{0.25}Al_2$. Although both the Tb^{3+} and Dy^{3+} ions have negative signs of Steven's factors, the magnitude of the factor for Tb^{3+} is much smaller $(-1/99)$ compared to $(-2/9.35)$ for Dy^{3+}, which means that the $4f$ charge density of the Tb^{3+} ion is much closer to a sphere. Therefore, the competition between the magnetoelastic coupling and quadrupolar terms in $Er_{0.25}Dy_{0.25}Al_2$ and $Er_{0.75}Tb_{0.25}Al_2$ are expected to be different. Due to the smaller magnitude of the Steven's factor of Tb^{3+} the competition is expected to be weaker in $Er_{0.75}Tb_{0.25}Al_2$ than it is in $Er_{0.25}Dy_{0.25}Al_2$. As a result, the peak in the ac susceptibility curve is weak for $Er_{0.75}Tb_{0.25}Al_2$ while it is much sharper for $Er_{0.25}Dy_{0.25}Al_2$. Another factor that may contribute to the weaker ac susceptibility anomalies and weaker heat-capacity peaks in $Er_{0.75}Tb_{0.25}Al_2$ is the difference in magnetic anisotropies of $Er_{0.75}Tb_{0.25}Al_2$ and $Er_{0.75}Dy_{0.25}Al_2$. Considering that in the ferromagnetic state the anisotropic exchange in RAl_2 compounds is small and can be neglected in most cases,[8] the contribution of the magnetic anisotropy in the aforementioned competition is likely small enough to be ruled out.

C. Magnetic relaxation studies

As was shown in Fig. 2, the FCW $M(T)$ curve of $Er_{0.75}Tb_{0.25}Al_2$ lies below the FCC $M(T)$ curve. A similar behavior was also observed in $Er_{0.75}Dy_{0.25}Al_2$ and in $(Er_{1-x}Gd_x)_5Si_4$ systems.[15,21] Usually, materials exhibiting such irreversibility in FCW and FCC $M(T)$ curves also demonstrate significant time dependence of their remanent magnetization. In order to explore if similar time dependence of remanent magnetization exists in $Er_{0.75}Tb_{0.25}Al_2$ we have performed isothermal magnetic relaxation measurements. Before each measurement the sample was cooled down from 200 K (paramagnetic state) to the measurement temperature in zero magnetic field. Once the desired temperature was reached a magnetic field of 100 Oe was applied to the sample for 1000 s. The magnetic field was then switched off, followed by the measurement of the magnetic relaxation as a function of time and the results are plotted in Fig. 6.

As shown in the Fig. 6, the magnetic relaxation exhibits strong time dependence. As the temperature is increased

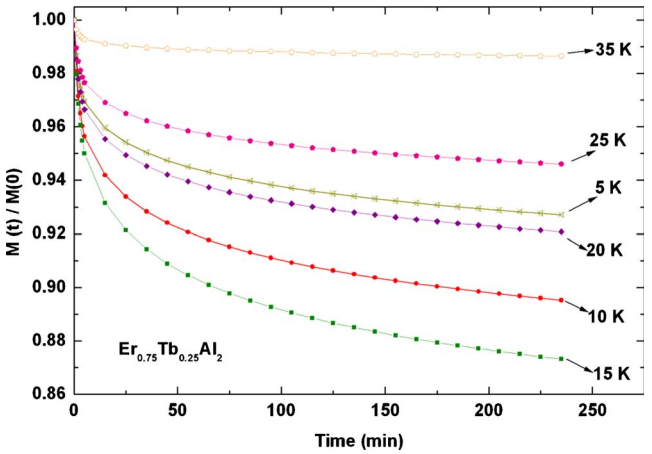

FIG. 6. (Color online) Remanent magnetization of $Er_{0.75}Tb_{0.25}Al_2$ measured as a function of time at different temperatures.

from 5 to 15 K the rate of the decay of the remanent magnetization increases, and as the temperature is increased above 15 K the rate begins to decrease. Each of the magnetic relaxation isotherms can be easily fitted to the following equation:

$$M(T,t) = M(T,0) - S(T)\ln(1+t), \quad (1)$$

where $M(T,t)$ is the remanent magnetization at temperature T and time t, $M(T,0)$ is the initial remanent magnetization, and $S(T)$ is the magnetic viscosity. The values $M(T,0)$ and $S(T)$ as functions of temperature are plotted in Fig. 7. Initially, $S(T)$ increases with increasing temperature, reaching a peak at 15 K. The $M(T,0)$ exhibits an opposite behavior to that of $S(T)$. With increasing temperature $M(T,0)$ decreases reaching a minimum at 15 K and then increases with increasing temperature.

The observed time dependence of the remanent magnetization in $Er_{0.75}Tb_{0.25}Al_2$ is similar to that observed in $Er_{0.75}Dy_{0.25}Al_2$,[15] and possible reasons behind such behavior were conjectured to be frustrations in the $4f$ exchange interactions in $Er_{0.75}Dy_{0.25}Al_2$ caused by the statistical distribution of Er^{3+} and Dy^{3+} ions in the crystal lattice. The observed magnetic relaxation behaviors in $Er_{0.75}Tb_{0.25}Al_2$ may also be attributed to similar frustrations, which in this case are caused by the random distributions of Er^{3+} and Tb^{3+} ions.

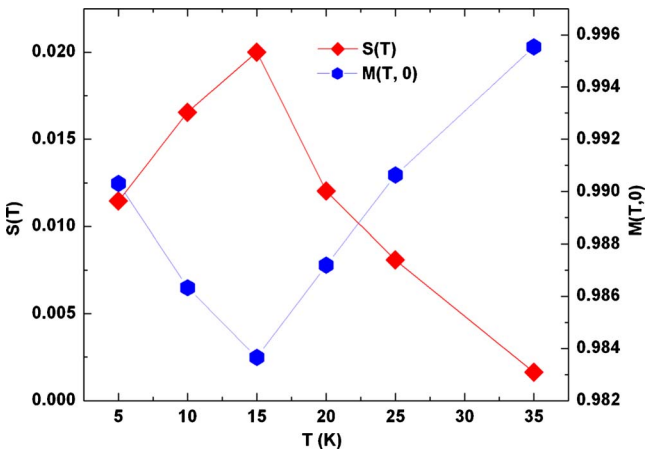

FIG. 7. (Color online) Magnetic viscosity and initial magnetization as a function of temperature of $Er_{0.75}Tb_{0.25}Al_2$.

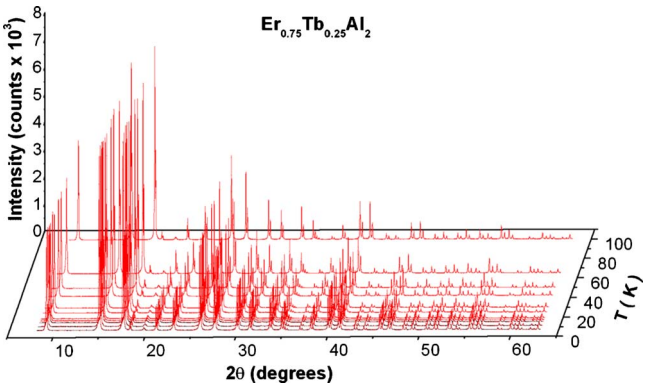

FIG. 8. (Color online) The powder x-ray diffraction patterns of $Er_{0.75}Tb_{0.25}Al_2$ measured at different temperatures.

D. Low-temperature XRD

As mentioned above, the $Er_{0.75}Tb_{0.25}Al_2$ alloy exhibits a transition with thermal hysteresis at 18 K (see Fig. 2). To further explore the nature of this transition we carried out temperature-dependent XRD measurements in zero magnetic field. The XRD measurements were performed at temperatures ranging from 5 to 300 K. The XRD patterns in the range from 5 to 100 K are shown in Fig. 8. In the entire temperature region, the $Er_{0.75}Tb_{0.25}Al_2$ alloy preserves the $MgCu_2$-type Laves phase structure (space group $Fd3m$). From the XRD measurements, no changes of the crystal structure were detected in the vicinity of the transition at 18 K. However, a steplike anomaly in the lattice parameter, typical for a first-order transition, was observed at 18 K as shown in Fig. 9. Above this transition the lattice parameter increases with increasing temperature with a minor fluctuation around T_C, where a slope change is observed. Above T_C

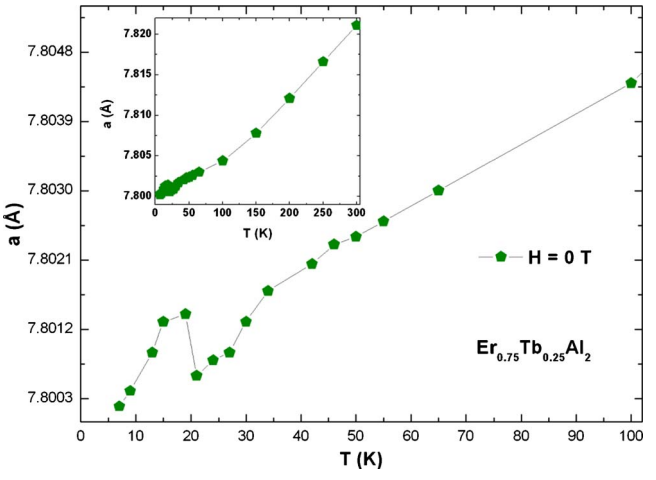

FIG. 9. (Color online) The lattice parameter a of $Er_{0.75}Tb_{0.25}Al_2$ as a function of temperature. The inset shows the same in the temperature range of 5–300 K.

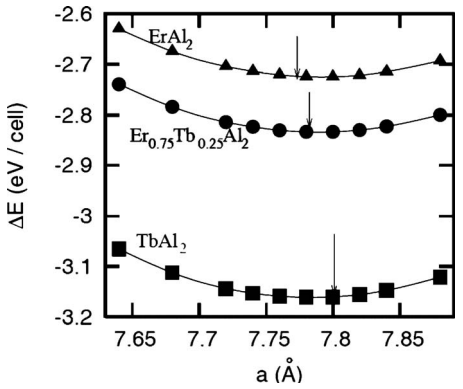

FIG. 10. Variation in the formation energies as functions of lattice parameter, a, in $TbAl_2$, $Er_{0.75}Tb_{0.25}Al_2$, and $ErAl_2$. The arrows show equilibrium lattice parameters.

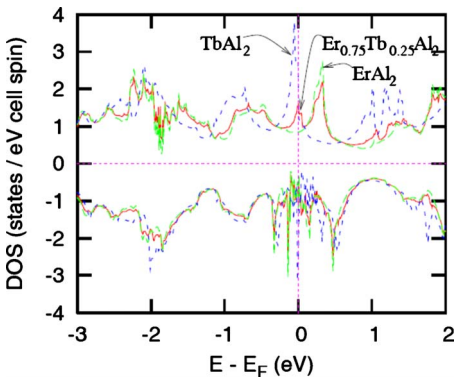

FIG. 11. (Color online) Conduction electron (*spd*) densities of states of $ErAl_2$, $Er_{0.75}Tb_{0.25}Al_2$, and $TbAl_2$ near the Fermi level.

the lattice parameter varies almost linearly with temperature. The slope changes around T_C are also evident in the thermal-expansion data of pure $ErAl_2$ and $DyAl_2$.[22] Such behaviors are common in the vicinity of second-order phase transitions and occur due to spontaneous magnetostriction of the material. At this point it appears that the low-temperature anomalies observed in $Er_{0.75}Tb_{0.25}Al_2$ and $Er_{0.75}Dy_{0.25}Al_2$ alloys occur due to strong magnetoelastic effects that are caused by lattice quadrupole coupling, although they do not facilitate a structural transformation.

IV. THEORETICAL INVESTIGATIONS

In order to gain an insight into the magnetism of $ErAl_2$, $Er_{0.75}Tb_{0.25}Al_2$, and $TbAl_2$ systems, first-principles electronic-structure calculations have been performed using the tight-binding linear muffin-tin orbital method[23] within the framework of the generalized gradient approximation (GGA) considering $4f$ electrons of Er and Tb as core electrons. The GGA+U approach[24,25] has also been applied and the results have been compared with the $4f$ core approach.

The formation energies of $ErAl_2$, $Er_{0.75}Tb_{0.25}Al_2$, and $TbAl_2$ are computed from the corresponding total energies and the formation energy of $TbAl_2$ is lowered by 0.44 eV/cell compared to $ErAl_2$. The formation energy of $Er_{0.75}Tb_{0.25}Al_2$ is also lowered by 0.33 eV/cell than that of the $ErAl_2$, which indicates that $Er_{0.75}Tb_{0.25}Al_2$ is energetically more favorable than $ErAl_2$. The equilibrium lattice parameters for $ErAl_2$, $Er_{0.75}Tb_{0.25}Al_2$, and $TbAl_2$ are 7.774 Å, 7.782 Å, and 7.801 Å, respectively, which are pointed out by arrows in Fig. 10. The change in equilibrium lattice constants is in accord with the lanthanide contraction. Here and below, the electronic-structure calculations for $Er_{0.75}Tb_{0.25}Al_2$ were performed by using the same volume but changing the cubic symmetry to $P1$ symmetry and locating Tb and Er atoms to match the concentration of Er and Tb atoms. Out of eight rare-earth sites in the $P1$ structure, six for Er and two for Tb atoms were randomly selected. The total-energy calculations with all possible permutations of Er and Tb positions show the same total energy indicating the insensitiveness in the selection of Er and Tb sites while matching the respective concentrations of Er and Tb atoms in $Er_{0.75}Tb_{0.25}Al_2$.

The spin-polarized conduction electron (*spd*) density of states (DOS) around the Fermi level for $TbAl_2$, $Er_{0.75}Tb_{0.25}Al_2$, and $ErAl_2$ compounds have been calculated and these are shown in the Fig. 11. There is a substantial spin polarization of the $5d$ states of Tb^{3+} in $TbAl_2$. The spin polarization of the $5d$ states of Tb^{3+} and Er^{3+} in the $Er_{0.75}Tb_{0.25}Al_2$ is much smaller compared to $TbAl_2$ while it is nearly zero for Er^{3+} in $ErAl_2$. This amounts to $\sim 0.21\ \mu_B$/Tb $5d$ magnetic moment in $TbAl_2$ but nearly zero (0.01 μ_B/Er $5d$) magnetic moment in $ErAl_2$. We note that the spin polarization in the $5d$ (conduction) electrons is a measure of the indirect $4f$-$4f$ exchange. Because of the Er content, the Ruderman-Kittel-Kasuya-Yoshida exchange is lower in $Er_{0.75}Tb_{0.25}Al_2$ compared to $TbAl_2$. The calculated $4f$ spin moments of Tb and Er in $Er_{0.75}Tb_{0.25}Al_2$ are 5.80 μ_B/Tb and 2.40 μ_B/Er, respectively. The calculations with GGA+U approach show 5.98 μ_B/Tb and 2.47 μ_B/Er $4f$ spin moments and 0.24 μ_B/Tb and 0.02 μ_B/Er $5d$ spin moments. The s and p moments are negligible. On the other hand the Hund's rule orbital moments are 3.0 μ_B/Tb and 6.0 μ_B/Er, respectively. This indicates that the orbital moment, which is directionally dependent and dominant in $ErAl_2$, has a substantial contribution in $Er_{0.75}Tb_{0.25}Al_2$. Because of this orbital moment contribution there is spin orbit coupling of 0.21 eV in Tb and 0.38 eV in Er.[26] The spin and orbital moment mismatch and spin-orbit coupling give rise to the competition between spin moments (mainly of Tb) and orbital moments (mainly of Er) in $Er_{0.75}Tb_{0.25}Al_2$

It is interesting to note that there is a small peak about 0.2 eV wide around the Fermi level in the DOS of $Er_{0.75}Tb_{0.25}Al_2$. Upon increasing the concentration of Er, the Fermi level moves to higher energy. On the other hand while increasing the concentration of Tb the Fermi level moves to the lower energy. This indicates that for some range of concentrations of Er close to 75% there is a peak at the Fermi level. This correlates very well with the low-temperature (~ 18 K) anomaly seen experimentally as explained above. It should be mentioned here that for pure $TbAl_2$ and $ErAl_2$ the peaks are below and above the Fermi level, respectively, but not at the Fermi level. This shows that pseudobinary $Er_{0.75}Tb_{0.25}Al_2$ behaves differently compared with binary

$TbAl_2$ and $ErAl_2$. DOS calculations for $Er_{0.25}Tb_{0.75}Al_2$ show that there is no peak at the Fermi level but the peak is located above the Fermi level indicating behavior similar to that of $TbAl_2$. Our calculations for $Er_{0.75}Dy_{0.25}Al_2$ show that there is a significant spin polarization on the 5*d* bands of Dy but negligible spin polarization on the 5*d* bands of Er, and the peculiar behavior around the Fermi level also exists for $Er_{0.75}Dy_{0.25}Al_2$.[27] This indicates that Tb and Dy have similar magnetic interactions with Er when a "magic" concentration of 25 at. % of Er is substituted either by Tb or Dy.

Since Tb and Er ions are randomly distributed in $Er_{0.75}Tb_{0.25}Al_2$ along with the spin-orbit coupling discussed above one should also consider crystal-field effects. Moreover, higher-order interactions such as quadrupolar interactions could play a vital role because the 4*f* charges of Er^{3+} and Tb^{3+} ions are nonspherical and they are prolate and oblate, respectively. The second-order Steven's coefficients, α_2 are negative for Tb and positive for Er and quadrupolar moments, $\frac{Q_2}{a_0^2}=\frac{\alpha_J\langle r^2\rangle_{4f}(2J^2-J)}{a_0^2}$ are −0.505 for Tb and 0.178 for Er estimated using the point-charge model.[28] Therefore the magnetic exchange, anisotropic spin-orbit, crystal-field and quadrupolar interactions could compete with each other at low temperatures and this competition could lead to a possible low-temperature anomaly seen in $Er_{0.75}Tb_{0.25}Al_2$. The perturbed angular correlation studies on the end member RAl_2 compounds have confirmed the strength of quadrupolar interactions in these systems.[29]

V. CONCLUSIONS

Magnetization measurements performed on the polycrystalline $Er_{0.75}Tb_{0.25}Al_2$ show that the alloy is ferromagnetic with a Curie temperature of 36 K. At 18 K the sample exhibits magnetic transition with thermal hysteresis suggesting the first-order nature of the transition. This transition also appears as a peak in the ac susceptibility data measured at 1 Hz. The peak almost disappears in frequencies higher than 1 Hz. From the low-temperature XRD measurements no structural transformations were identified. This behavior is also supported by the results of total-energy calculations. Anomalies in the lattice parameters are observed in the vicinity of the first-orderlike transition at 18 K. These anomalies are also reflected in the DOS of $Er_{0.75}Tb_{0.25}Al_2$ where unusual peak is observed at the Fermi level. The results for the title system are similar to the results of the previously reported $Er_{0.75}Dy_{0.25}Al_2$ alloy. The similarity in the experimental results strengthens the assumption that mixing two rare earth ions with opposite signs of second-order Steven's factors in RAl_2 alloys causes an enhancement of quadrupolar interactions resulting in the appearance of first-order phase transitions in the pseudobinary RAl_2 alloys.

ACKNOWLEDGMENTS

The Ames Laboratory is operated for the U.S. Department of Energy by Iowa State University of Science and Technology under Contract No. DE-AC02-07CH11358. This work was supported by the Office of Basic Energy Sciences, Materials Sciences Division of the U.S. DOE.

[1] F. Pourarian and W. E. Wallace, J. Appl. Phys. **50**, 7707 (1979).
[2] T. Hashimoto, T. Kuzuhara, M. Sahashi, K. Inomata, A. Tomokiyo, and H. Yayama, J. Appl. Phys. **62**, 3873 (1987).
[3] F. W. Wang, X. X. Zhang, and F. X. Hu, Appl. Phys. Lett. **77**, 1360 (2000).
[4] K. A. Gschneidner, Jr., H. Takeya, J. O. Moorman, and V. K. Pecharsky, Appl. Phys. Lett. **64**, 253 (1994).
[5] J. C. P. Campoy, E. J. R. Plaza, A. A. Coelho, and S. Gama, Phys. Rev. B **74**, 134410 (2006).
[6] H. G. Purwins, E. Walker, B. Barbara, M. F. Rossignol, and P. Bak, J. Phys. C **7**, 3573 (1974).
[7] N. Kaplan, E. Dormann, K. H. J. Buschow, and D. Lebenbaum, Phys. Rev. B **7**, 40 (1973).
[8] H. G. Purwins and A. Leson, Adv. Phys. **39**, 309 (1990).
[9] M. R. Ibarra, O. Moze, P. A. Algarabel, J. I. Arnaudas, J. S. Abell, and A. del Moral, J. Phys. C **21**, 2735 (1988).
[10] P. J. von Ranke, N. A. de Oliveira, D. C. Garcia, V. S. R. de Sousa, V. A. de Souza, A. M. G. Carvalho, S. Gama, and M. S. Reis, Phys. Rev. B **75**, 184420 (2007).
[11] K. W. H. Stevens, Proc. Phys. Soc., London, Sect. A **65**, 209 (1952).
[12] W. M. Swift and W. E. Wallace, J. Phys. Chem. Solids **29**, 2053 (1968).
[13] K. A. Gschneidner, Jr., V. K. Pecharsky, and S. K. Malik, Adv. Cryog. Eng. **42**, 475 (1996).
[14] A. L. Lima, K. A. Gschneidner, Jr., V. K. Pecharsky, and A. O. Pecharsky, Phys. Rev. B **68**, 134409 (2003).
[15] R. Nirmala, Ya. Mudryk, V. K. Pecharsky, and K. A. Gschneidner, Jr., Phys. Rev. B **76**, 014407 (2007).
[16] M. Khan, K. A. Gschneidner, Jr., and V. K. Pecharsky, Phys. Rev. B **80**, 224408 (2009).
[17] Materials Preparation Center, Ames Laboratory US-DOE, Ames, IA, USA, www.mpc.ameslab.gov
[18] A. P. Holm, V. K. Pecharsky, and K. A. Gschneidner, Jr., Rev. Sci. Instrum. **75**, 1081 (2004).
[19] Ya. Mudryk, A. P. Holm, K. A. Gschneidner, Jr., and V. K. Pecharsky, Phys. Rev. B **72**, 064442 (2005).
[20] B. Hunter, IUCR Comm. Powder Diff. Newsl. **20**, 21 (1998).
[21] N. K. Singh, V. K. Pecharsky, and K. A. Gschneidner, Jr., Phys. Rev. B **77**, 054414 (2008).
[22] K. Kamiya, T. Numazawa, T. Koen, T. Okano, and K. Matsumoto, Adv. Cryog. Eng. **50**, 11 (2004).
[23] O. K. Andersen and O. Jepsen, Phys. Rev. Lett. **53**, 2571 (1984).
[24] V. I. Anisimov, F. Aryasetiawan, and A. I. Liechtenstein, J. Phys.: Condens. Matter **9**, 767 (1997).
[25] B. N. Harmon, V. P. Antropov, A. I. Liechtenstein, I. V. Solovyev, and V. I. Anisimov, J. Phys. Chem. Solids **56**, 1521 (1995).

[26] S. Lebègue, A. Svane, M. I. Katsnelson, A. I. Lichtenstein, and O. Eriksson, J. Phys.: Condens. Matter **18**, 6329 (2006).
[27] R. Nirmala, D. Paudyal, V. K. Pecharsky, and K. A. Gschneidner, Jr., J. Appl. Phys. **107**, 09A723 (2010).
[28] R. Skomski, *Simple Models of Magnetism* (Oxford University Press, New York, 2006), Chap. 3, p. 94.
[29] P. de la Presa, M. Forker, J. Th. Cavalcante, and A. P. Ayala, J. Magn. Magn. Mater. **306**, 292 (2006).